scientific reports

Check for updates

OPEN

Tensile modulus of polymer halloysite nanotubes nanocomposites assuming stress transferring through an imperfect interphase

Yasser Zare[1]✉, Muhammad Tajammal Munir[2] & Kyong Yop Rhee[3]✉

In this work, Hui-Shia model is developed to reveal the efficiency of a deficient interphase on the tensile modulus of polymer halloysite nanotube (HNT) nanocomposites. "L_c" as essential HNT length providing full stress transferring is defined and effective HNT size, effective HNT concentration, and efficiency of stress transferring (Q) are expressed by "L_c". Furthermore, the influences of all terms on the "Q" and nanocomposite's modulus are clarified, and also the calculations of the model are linked to the tested data of some nanocomposites. Original Hui-Shia model overpredicts the moduli, but the innovative model's predictions appropriately fit the measured data. L_c = 200 nm maximizes the sample's modulus to 2.6 GPa, but the modulus reduces to 2.11 GPa at L_c = 700 nm. Therefore, there is a reverse relation between the sample's modulus and "L_c". Q = 0.5 produces the system's modulus of 2.1 GPa, while the modulus of 2.35 GPa is achieved at Q = 1 providing a direct relation between the nanocomposite's modulus and "Q". Generally, narrow and big HNTs, along with a low "L_c", enhance the "Q", because a lower "L_c", reveals a tougher interphase improving the stress transferring.

Keywords Halloysite nanotubes, Polymer nanocomposites, Tensile modulus, Stress transferring

Alumina-silicates and tubular halloysite nanotubes (HNTs) are desirable for high reinforcing of polymer media, because the small area of inter-tubular contacts guarantees the HNT dispersion[1–6]. HNTs have a length of 0.3–2 μm, an inner diameter of 15–100 nm, and an external diameter of 40–120 nm[7]. Also, HNTs as one dimensional (1D) natural nanomaterial have unique anisotropic properties including ionic conductivity, optical and dielectric features[8]. HNT exhibits many attractive advantages including higher biocompatibility, better solubility in water, environmental friendliness, as well as natural occurring[9]. Therefore, they are attractive on several areas due to the extraordinary performance and inexpensive cost. Hydroxyl groups on the external layer of HNTs increase the hydrophobicity and fine dispersion in the polymer medium[10]. However, the microparticles do not produce the big surface area involving the polymer chains[11–14]. Moreover, the interfacial interactions among the polymer and micro-particles are not strong declining the reinforcing. In addition, the natural modulus/strength of nanoparticles like HNT is much higher than the micro-particles and HNT has a low density reducing the weight of nanocomposites. Hence, HNTs are better than microparticles for the reinforcing of polymer mediums.

In contrast to carbon nanotubes (CNTs) and graphene, HNTs are naturally-occurring clay minerals readily available in abundance. HNTs are low-cost, and eco-friendly materials that can be more effortlessly dispersed in a polymer medium than CNTs[15]. Moreover, HNTs have high aspect ratio, high resistance to heat and chemical substances, and relatively low density. Since HNTs are naturally occurring and much cheaper, yet morphologically similar to CNTs, the HNTs can be a substitute for more expensive CNTs.

HNTs can improve the fracture toughness of epoxy without deteriorating the modulus, strength, and thermal balance[16]. Also, HNTs increase the crystallinity and crystallization temperature of polyamide-11 composites[17]. Many researchers have found that HNTs improve the performances of polymer composites[3,5,6,18].

[1]Biomaterials and Tissue Engineering Research Group, Department of Interdisciplinary Technologies, Breast Cancer Research Center, Motamed Cancer Institute, ACECR, Tehran, Iran. [2]College of Engineering and Technology, American University of the Middle East, Egaila 54200, Kuwait. [3]Department of Mechanical Engineering (BK21 four), College of Engineering, Kyung Hee University, Yongin, Republic of Korea. ✉email: y.zare@aut.ac.ir; rheeky@khu.ac.kr

However, models for the properties of HNT-based composites are incomplete. It should be noted that previous investigations have concentrated on the experimental analyses of this system because HNTs are a new type of multifunctional nanofiller, progressing the numerous characteristics of polymer media.

Nanocomposites encompass an interphase zone between polymer media and nanofillers due to the immense surface zone of the nanoparticles[19–26]. Actually, the big surface area of nanoparticles and the strong interaction/adhesion between the polymer and nanoparticle produce a different phase around the nanoparticles named as interphase zone. Many studies evaluated the interphase properties by the mechanical performance and conductivity of the nanocomposites[27–34]. Usually, a dense/tough interphase advantageously strengthens the composites. Meanwhile, it supports the load transported from the polymer media to the particles[28,29,35]. It was stated that polymer nanocomposites regularly encompass an imperfect interphase because polymer matrices have poor compatibility with nanofillers in most cases[36,37]. Therefore, the interphase section is not strong enough to shift a high load from a medium to a filler; thus, the defective interphase partly transfers the stress. "L_c" is the required filler length to provide successful stress shifting. "L_c" has previously been reflected as the smallest filler length allowing operative stress transferring[38,39]. Therefore, a filler length of more than "L_c" provides good stress transfer, thus reinforcing the nanocomposites, while a filler length smaller than "L_c" cannot provide stress, thus weakening the system. This explanation reveals that "L_c" significantly affects the effective aspects of nanoparticles in nanocomposites because "L_c" controls the stress flow and strengthening success. However, former models usually did not consider the faulty interphase and "L_c" in nanocomposite mechanics.

Hui-Shia model[40] considers the perfect interface between polymer and filler in the composites. Consequently, it cannot estimate the nanocomposite modulus when the interface/interphase is imperfect. Actually, it is necessary to develop Hui-Shia model considering an imperfect interphase in nanocomposites. The hypothesis of the interphase section in a HNT-based system is essential because the interphase zone controls the performance of composites. The thickness of interphase is defined at the round of HNTs and varies from the surface of nanoparticles to nearby polymer matrix. The interphase thickness does not relate to the volume fraction of HNTs, but the interfacial adhesion between HNT and polymer matrix affects the interphase thickness. Considering the interphase section enhances the accuracy of a model for predicting the nanocomposite's performance.

Some papers have studied the prediction of tensile modulus for polymer nanocomposites containing HNTs below and after mechanical percolation[5,19,41,42]. The models before mechanical percolation assumed the dispersion of all nanoparticles in the system, but the networking of both HNT and surrounding interphase was supposed after mechanical percolation. However, the mentioned models have reflected the perfect interphase around the HNT, but they neglected the imperfect interphase weakening the stress transferring. In this article, the modulus of HNT-based samples is analyzed below mechanical percolation assuming the imperfect interphase. The nanocomposite characteristics such as operative aspect ratio and operational HNT concentration are expressed by "L_c". Moreover, "Q" as the efficiency of load moving by interphase is defined. Furthermore, Hui-Shia model is developed by the stated terms to take the deficient interphase and the stiffness of HNT sample into account. The established model efficiently reflects the effectiveness' of HNT size, interfacial shear modulus, "L_c" and stress transfer efficiency on the stiffness. The roles of all factors in the efficiency of stress transferring and the modulus of the system are plotted and explained. Moreover, calculations of established techniques are connected to the experimental data of various nanocomposites, and the mentioned terms are estimated for the samples. All parameters and equations are meaningful and reasonable enabling the modulus prediction for the HNT-filled systems.

Equations

"L_c" is the lowest filler length, which is crucial to reach the normal stress to the supreme filler's modulus, initiating the effective stress shifting via an interphase piece[38].

"L_c" has previously been expressed for CNT-based examples[43], which is also valid for HNT-filled materials:

$$L_c = \frac{E_f R}{G_i} \tag{1}$$

Here "E_f" is the HNT modulus, "R" is the HNT radius and "G_i" is the interfacial shear modulus. As mentioned, a HNT length smaller than $2L_c$ cannot deliver stress transferring, but a HNT length of more than $2L_c$ enables stress conveyance.

Assuming the definition of "L_c" for stress transferring and HNT length, a parameter for the efficiency of stress transfer can be given by:

$$Q = \frac{l}{4L_c} \tag{2}$$

Here "l" is the HNT length. "Q" demonstrates a criterion for the extent of stress transferring in nanocomposites. When $l = 2L_c$, HNT cannot provide the stress transferring. So, $Q = 1/2$ reveals no stress transferring through the imperfect interphase. However, $Q > 1/2$ can provide the stress transferring via the imperfect interphase reinforcing the system. "Q" implicitly expresses the amount of interfacial bonding, because the stress moving via the interphase directly associates with the interfacial connections.

Inserting "L_c" from Eq. (1) into Eq. (2) causes:

$$Q = \frac{G_i l}{4E_f R} \tag{3}$$

which correlates the "Q" to the "G_i" and HNT characteristics.

The defective interfacial bonding weakens the operational opposite aspect ratio (α_{eff}) and operative volume portion (φ_{eff}) of particles in the samples[44].

"α_{eff}" and "φ_{eff}" were suggested in CNT examples[44] appropriate for HNT-filled system as:

$$\alpha_{eff} = \alpha(\frac{8L^2{}_c}{l^2} + 1) \tag{4}$$

$$\varphi_{eff} = \varphi_f[\frac{1}{2} + (\frac{l - 2L_c}{l^2})(l - L_c)] \tag{5}$$

where "α" as 2R/*l* is the reverse aspect ratio and "φ_f" is the volume portion of HNTs in the material.

Rearranging of Eq. 2 results in an equation for "L_c" as a function of "Q" as:

$$L_c = \frac{l}{4Q} \tag{6}$$

If "L_c" in Eqs. 4 and 5 is replaced by Eq. 6, "α_{eff}" and "φ_{eff}" are linked to "Q" by:

$$\alpha_{eff} = \alpha(\frac{1}{2Q^2} + 1) \tag{7}$$

$$\varphi_{eff} = \varphi_f[\frac{1}{2} + (1 - \frac{1}{2Q})(1 - \frac{1}{4Q})] \tag{8}$$

which easily associate the effective terms to "Q".

The mentioned terms for the defective interfacial attachment in the HNT-reinforced system are applied to expand the Hui-Shia model.

Hui-Shia model[40] reflects the perfect interfacial connection among polymer matrix and particles in the nanocomposite's modulus. Also, this model considers the aspect ratio of filler, which is important for the nanocomposites containing long and thin nanoparticles such as HNTs. Actually, original Hui-Shia model cannot consider the imperfect interphase in the nanocomposites and we developed this model to estimate the modulus of HNT-filled samples.

Hui-Shia model is expressed by:

$$E_{11} = \frac{E_m}{1 - \frac{\varphi_f}{A}} \tag{9}$$

$$E_{22} = \frac{E_m}{1 - \frac{\varphi_f}{4}(\frac{1}{A} + \frac{3}{A+B})} \tag{10}$$

$$A = \varphi_f + \frac{E_m}{E_f - E_m} + 3(1 - \varphi_f)[\frac{(1 - g)\alpha^2 - \frac{g}{2}}{\alpha^2 - 1}] \tag{11}$$

$$B = (1 - \varphi_f)[\frac{3(\alpha^2 + 0.25)g - 2\alpha^2}{\alpha^2 - 1}] \tag{12}$$

$$g = \frac{\pi}{2}\alpha \tag{13}$$

in which "E_{11}" and "E_{22}" denote the longitudinal and transverse moduli of composites, correspondingly, and "E_m" is the polymer medium modulus.

"A" and "B" in the Hui-Shia equation can be modified supposing the features of HNT. HNT features include high stiffness (140 GPa[45]) and a short reverse aspect ratio (α = 60/1500 = 0.04 when *R* = 30 nm and *l* = 1500 nm). So, $E_f - E_m >> E_m$ and $\alpha^2 \approx 0$. These comments simplify A (Eq. 11) and B (Eq. 12) as:

$$A = \varphi_f + 3(1 - \varphi_f)(\frac{g}{2}) \tag{14}$$

$$B = (1 - \varphi_f)(-0.75g) \tag{15}$$

If "α_{eff}" and "φ_{eff}" for the incomplete interfacial attachment between the polymer host and HNTs are inserted in the Hui-Shia model (Eqs. 9–13), the simplified model is given by:

$$E_{11} = \frac{E_m}{1 - \frac{\varphi_{eff}}{A_{eff}}} \tag{16}$$

$$E_{22} = \frac{E_m}{1 - \frac{\varphi_{eff}}{4}(\frac{1}{A_{eff}} + \frac{3}{A_{eff}+B_{eff}})} \tag{17}$$

$$A_{eff} = \varphi_{eff} + 3(1 - \varphi_{eff})(\frac{g}{2}) \tag{18}$$

$$B_{eff} = (1 - \varphi_{eff})(-0.75g) \tag{19}$$

$$g = \frac{\pi}{2}\alpha_{eff} \tag{20}$$

which correlate the various moduli of the system to the effective terms.

If "α_{eff}" (Eq. 4) and "φ_{eff}" (Eq. 5) are used in the latter equations, the simplified model considers the role of "L_c" in the modulus of the system. Also, substituting "α_{eff}" and "φ_{eff}" from Eqs. (4) and (5) into Eqs. (16)–(20) enables the estimation of the nanocomposite's moduli by "Q".

The modulus of a sample comprising randomly 3D arranged HNTs is calculated[46] by:

$$E = 0.49E_{11} + 0.51E_{22} \tag{21}$$

which reflects the contributions of longitudinal and transverse moduli in the modulus of a nanocomposite.

"φ_f" is calculated by the weight fraction of nanofiller in nanocomposites (w_f) as:

$$\varphi_f = \frac{d_c}{d_f} w_f \tag{22}$$

$$d_c = \frac{d_m d_f}{(1 - w_f)d_f + w_f d_m} \tag{23}$$

where "d_c", "d_f" and "d_m" are the density of nanocomposite, HNTs and polymer medium, respectively.

Results and discussion

Examination of "Q"

The effects of various features on the "Q" factor (Eqs. 2 and 3) are plotted in Fig. 1. Each plot demonstrates the impact of one factor on the "Q" at the middling points of the variables. The average/constant values of the factors are supposed as $l = 1500$ nm, $E_f = 140$ GPa[45], $R = 30$ nm, and $G_i = 10$ GPa as the average value obtained from Table 1.

Figure 1a shows the character of "R" in the "Q" using Eq. (3). A low value of "R" enhances the "Q", but "Q" weakens at high values of "R". Consequently, narrow HNTs are appropriate to grow the "Q". In contrast, thick HNTs undesirably decrease the "Q". This relation is meaningful because skinny HNTs enlarge the surface area and

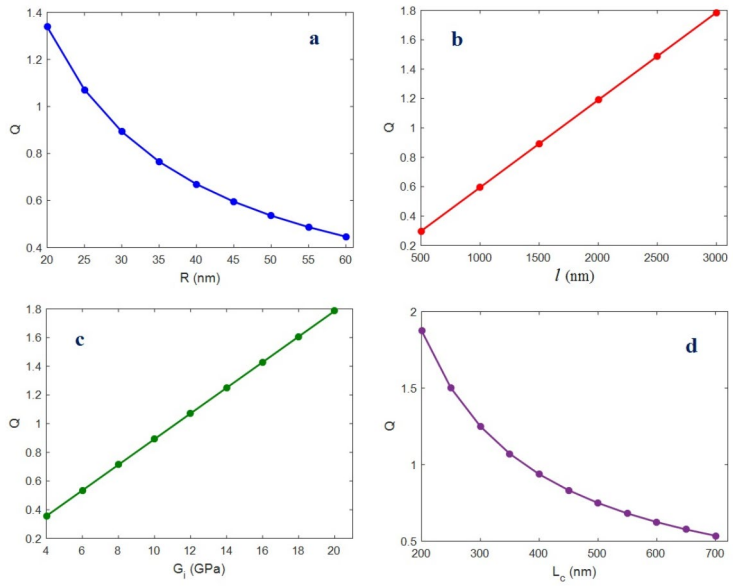

Fig. 1. The calculations of "Q" at many series of (**a**) HNT radius, (**b**) length of HNT, (**c**) interfacial shear modulus and (**d**) "L_c" using Eqs. (2) and (3).

Samples [Ref.]	E_m (GPa)	*R* (nm)	l (nm)	E_f (GPa)	G_i (GPa)	L_c (nm)	Q
PA6/HNTs[49]]	2.80	30	1500	140	8.50	494.1	0.76
PA610/HNTs[50]	2.00	30	1500	140	9.50	442.1	0.85
PVA/HNTs[51]	0.25	25	1200	140	12.5	280.0	1.07
PLA/HNTs[52]	1.72	30	1500	140	9.00	466.7	0.80

Table 1. Characteristics of various HNT-reinforced nanocomposites.

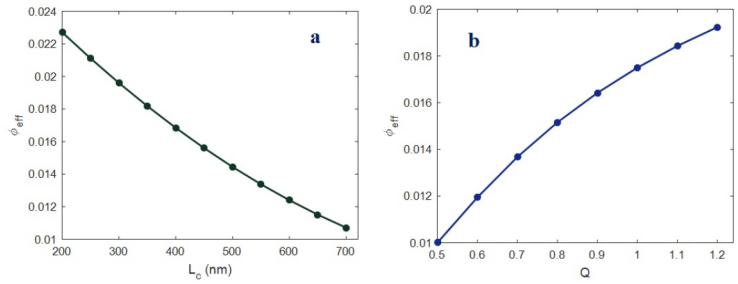

Fig. 2. Dependence of the effective volume portion of HNTs on the (**a**) "L_c" and (**b**) "Q" using Eqs. (5) and (8).

interphase section. Meanwhile, a big interphase strengthens the stress shifting[47,48], and skinny HNTs reasonably increase the effective stress moving and "Q". However, thicker HNTs abbreviate the interface/interphase section and limit the stress shifting. So, a smaller "Q" is expected with denser HNTs, confirming the correction of the suggested equation.

Figure 1b demonstrates the variation of "Q" at various ranges of HNT length (Eq. 3). "Q" is 0.3 at $l = 500$ nm, but "Q" improves to 1.79 at $l = 3000$ nm. "Q" directly correlates to HNT length, and larger HNTs produce the higher "Q". This observation can be explained by the simple notion that the larger HNTs provide a big surface area and numerous connections between polymer chains and particles. The high interactions cause a high amount of stress transferring, thus growing the "Q". In contrast, short HNTs have a low surface area causing few connections between polymer chains and nanofillers. Consequently, short HNTs yield poor stress shifting, therefore deteriorating the "Q". This evidence proves the suitability of Eq. 3 to accurately describe "Q".

Figure 1c establishes a link between "Q" and "G_i" according to Eq. (3). $G_i = 4$ GPa produces a "Q" of 0.38, whereas $G_i = 20$ GPa maximizes "Q" to 1.8. This plot shows that the interfacial shear modulus directly correlates to "Q". A higher value of the interfacial shear modulus results in a stronger interphase in the system, and the extent of stress shifting increases with a stronger interphase. Accordingly, a greater interfacial shear modulus produces a bigger "Q". In contrast, a negligible interfacial shear modulus results in a faintness of the interphase for stress moving, reducing the "Q". Hence, it can be concluded that the interfacial shear modulus directly controls "Q," supporting Eq. (3).

Figure 1d represents the correlation of "Q" to "L_c" using Eq. (2). A shorter "L_c" produces a higher "Q", but the "Q" decreases at high "L_c", establishing an inverse link between "Q" and "L_c". This correlation is also correct because a short "L_c" results in a stronger interphase, easing the stress moving. At the same time, a larger "L_c" results in a weakness of the interphase section, reducing the stress transfer. There is an inverse relationship between "Q" and "L_c", because a higher "Q" demonstrates a higher efficiency of stress transferring, which is obtained at lower "L_c". Conversely, a low "Q" shows inefficient stress shifting through the interphase section, which validates the high level of "L_c". As a result, it can be concluded that Eq. (2) indeed associates the "Q" with "L_c" in the current system.

Examination of effective HNT concentration

The roles of "L_c" and "Q" in the effective volume portion of HNTs (φ_{eff}) are plotted according to Eqs. (5) and (8) at constant $\varphi_f = 0.02$ and $l = 1500$ nm in Fig. 2. As shown in Fig. 2a, $L_c = 200$ nm maximizes the "φ_{eff}" to 0.023, but $L_c = 700$ nm reduces the "φ_{eff}" to about 0.011. Therefore, "L_c" adversely manipulates the "φ_{eff}", and to achieve a higher value for the effective HNT volume portion, it is necessary to shorten the "L_c". This occurrence is expected because a lower "L_c" reveals the development of a sturdier interphase in the system, which significantly strengthens the nanocomposites. In contrast, a high "L_c" displays a weak interphase, which is ineffective on the system's stiffness. It is assumed that the stiffening efficiency of HNTs directly associates with the modulus of the interphase section. Consequently, a tougher interphase represents a smaller "L_c" and grows the efficiency of HNT concentration. In contrast, a poorer interphase causes a larger "L_c" and diminishes the HNT efficiency for reinforcing. These findings verify the suggested equation.

Figure 2b depicts the role of "Q" in "φ_{eff}" based on Eq. 8. $Q = 0.5$ results in a low "φ_{eff}" of 0.01, but at $Q = 1.2$, "φ_{eff}" increases to 0.019. These results demonstrate that "Q" directly controls the "φ_{eff}" in the system. An excellent range of "Q" exhibits high interphase efficiency for stress moving, which increases the reinforcing efficiency of HNTs in the samples. However, a small "Q" reveals poor stress transferring due to the weak

interphase, which depreciates the efficiency of HNTs in the samples. As mentioned, the nanoparticle's efficiency correlates to the extent of interphase strength/modulus because both HNT and the adjoining interphase simultaneously strengthen the samples. A higher "Q" represents the significant efficiency of the interphase for load carrying, which clearly validates the significant efficiency of nanoparticles in the samples. Therefore, Eq. 8 correctly relates "φ_{eff}" to "Q" in the HNT-filled system.

Comparison of models' predictions with experimental facts

Here, the estimations of the old and progressed models are linked to the tested data of some specimens from published papers[49–52]. Table 1 shows the samples and their properties as found in the original references. The studied samples are nanocomposites, because the radius of HNT was reported from 25 nm to 30 nm. Additionally, the spacing between the HNT in the nanocomposites is not high to exceed the nanoscale. The HNT modulus is 140 GPa, according to the results reported in[45]. Figure 3 compares the tested and theorized results for the examples. The Hui-Shia model expectedly overpredicts the moduli of samples since it undertakes the complete interfacial bonding between HNTs and medium.

In contrast, the model calculations assume the imperfect interphase correctly and therefore, accurately follow the experimental data. The acceptable agreements among the tested values and the hypothetical data of the advanced model reveal that the progressive model can accurately predict the modulus of the examples.

Table 1 demonstrates the values of "G_i" calculated by the advanced model. The maximum "G_i" is obtained for the PVA/HNTs sample, while the PA6/HNTs system shows the lowest "G_i". "G_i" and the HNT radius are inserted into Eq. (1) to approximate "L_c" for the examples. "L_c" varies from 280 to 494.1 nm for the examples. The smallest and the largest "L_c" are detected in the PVA/HNTs and PA6/HNTs nanocomposites, respectively. The "L_c" and "l" values are substituted into Eq. (3) to predict the "Q". "Q" changes from 0.76 to 1.07 for the current products. The maximum and smallest levels of "Q" occur in the PVA/HNTs and PA6/HNTs samples, correspondingly. The values of "G_i", "L_c", and "Q" reveal that the sturdiest interphase and the most compatibility between polymer matrix and nanofiller are obtained in the PVA/HNTs system. At the same time, PA6/HNTs nanocomposite contains the poorest interphase zone based on these calculations.

Assuming the reported results in Fig. 3, the PVA/HNTs nanocomposite (Fig. 3c) shows the biggest modulus improvement compared to the other samples. Meanwhile, the PA6/HNTs system (Fig. 3a) presents the poorest modulus because the modulus of the nanocomposite improves to 5.3 GPa at 30 wt% HNTs (E_m = 2.8 GPa). The PVA and PA6 samples display the highest and the lowermost increments in the modulus, which cause the strongest and the weakest interphases, respectively. Accordingly, the advanced model accurately considers the reinforcing usefulness of the interphase in the samples. Moreover, all calculations for "G_i", "L_c" and "Q" determine the same trend among interfacial/interphase terms. In other words, the PVA/HNTs system displays the highest "G_i" and "Q" and the lowermost "L_c" among the samples. The accurate calculations of "G_i", "L_c", and "Q" for the current systems approve the suitability of the advanced model.

Analyses of advanced model

All factors in the advanced model are evaluated by plotting their contributions to the modulus of the system. A plot shows the effect of a parameter on the nanocomposite's modulus at standard ranks of other issues. The typical ranges of factors are φ_f = 0.02, l = 1500 nm, E_f = 140 GPa[45], E_m = 2 GPa, G_i = 10 GPa, and R = 30 nm. The plotted schemes determine the modulus of samples at several series of factors.

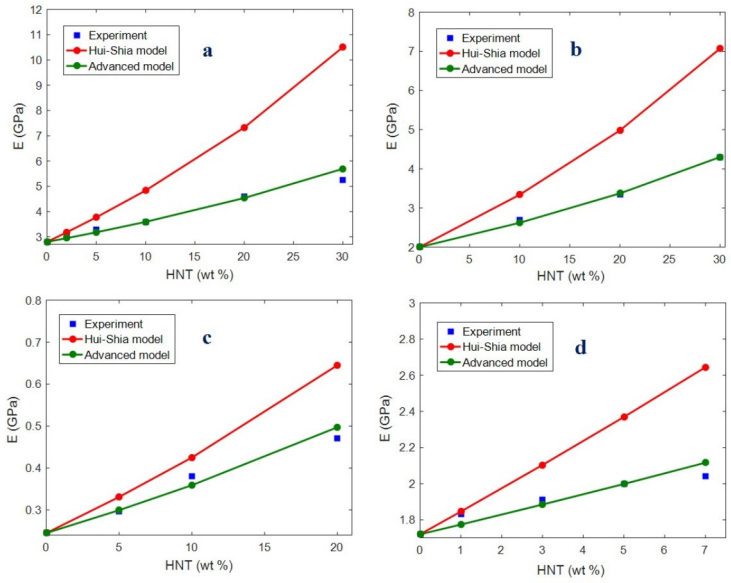

Fig. 3. Experimental and calculated moduli by old and progressed models for HNT-based (**a**) PA6[49], (**b**) PA610[50], (**c**) PVA[51], and (**d**) PLA[52] examples.

Figure 4 shows the impact of "L_c" on the system's modulus. L_c = 200 nm harvests a modulus of 2.6 GPa. Nonetheless, the modulus reduces to 2.11 GPa at L_c = 700 nm. The results demonstrate an inverse link between the modulus of the samples and "L_c". They indicate that a shorter "L_c" causes a more robust system, while a higher "L_c" diminishes the stiffness of the HNT-filled system. Indeed, the lowest rank of "L_c" is optimal for achieving the system's highest reinforcement. The nanocomposite modulus inconsistently links to the "L_c" because the modulus of the system linearly reduces at L_c < 500 nm, but it is relatively constant at too high "L_c".

A shorter "L_c" establishes a higher proficiency of the interphase for tension bearing and moving[38,39]. A lower "L_c" displays a stronger interphase, which transports a higher amount of stress. Clearly, the sample includes a higher modulus in this condition because a tougher interphase endures and shifts a higher amount of stress. In comparison, a big "L_c" reveals the creation of a poor interphase in the samples. A weak interphase cannot tolerate a high volume of tension and fades easily, which fails the modulus of material. It can be said that a high "L_c" undesirably lessens the modulus since it deteriorates the tension carrying via an interphase piece. Accordingly, the advanced model appropriately links the composite's modulus to "L_c".

Figure 5 demonstrates the character of "Q" in the modulus by the innovative model. Q = 0.5 introduces a modulus of 2.1 GPa, though the maximum stiffness is 2.35 GPa at Q = 1. Therefore, "Q" directly manipulates the modulus of the materials and a greater "Q" is essential to upsurge the modulus of the system. It can be said that the modulus of the samples linearly associates with "Q", and that the modulus constantly increases as "Q" enhances.

A higher "Q" results in more efficient stress transfer via the interphase piece, which positively controls the reinforcing of the system. A nanocomposite needs a robust interphase for transferring of stress. A higher "Q" exhibits increased effectiveness of the interphase for stress-bearing, which grows the modulus of the materials. Conversely, a low "Q" results in the creation of a weak interphase, which easily breaks during loading and cannot tolerate tension. A lower "Q" shows less efficiency of the interphase section for stress transfer, which makes a weaker nanocomposite. This evidence confirms the direct link between the rigidity of examples and "Q", as mentioned by the model.

In Fig. 6, the variation of the system's modulus by "G_i" is plotted. The minimum "G_i" of 4 GPa harvests a modulus of 2.05 GPa. Nonetheless, the stiffness reaches 2.58 GPa at G_i = 20 GPa. A higher interfacial shear modulus produces a higher stiffness of the system. Hence, there is a direct relationship between the stiffness and the interfacial shear modulus. The nanocomposite's modulus linearly increases with an interfacial shear modulus of G_i < 14 GPa, but higher levels of the interfacial shear modulus have a poor effect on the modulus of the system. Generally, it is essential to maximize the interfacial shear modulus to obtain a stiffer system.

A higher value of the interfacial shear modulus represents a stronger interphase in the system, intensifying the reinforcing. An excellent interfacial shear modulus expresses the desirable characteristics of the interphase section, which results in a high reinforcing efficiency. In comparison, a negligible interfacial shear modulus displays the feebleness of the interphase section, which consequently cannot reinforce the samples. Indeed, a poor interphase with a low interfacial shear modulus has a poor influence on the reinforcing of the nanocomposites because the interphase is not tough enough to reinforce the large volume of the weak polymer matrix. Based on this explanation, "G_i" directly controls the system's modulus certifying the innovative model.

Figure 7 depicts the calculations of the nanocomposite's modulus at numerous HNT weight proportions. The average densities of HNTs and the polymer medium are presumed as 2.5 and 1 g/cm, correspondingly. The highest concentration of HNTs produces the maximum modulus. The modulus of the system reaches 2.65 GPa by 10 wt% HNTs. As a result, a higher amount of HNTs is more desirable for reinforcing the nanocomposites.

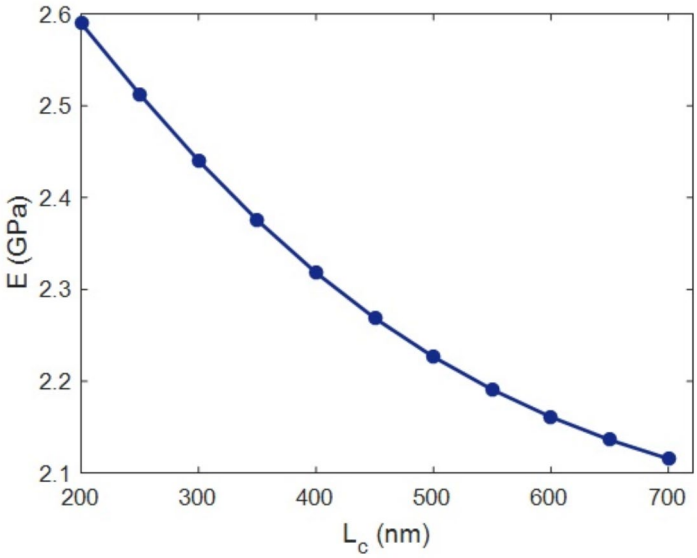

Fig. 4. The calculations of the composite's modulus at various levels of "L_c".

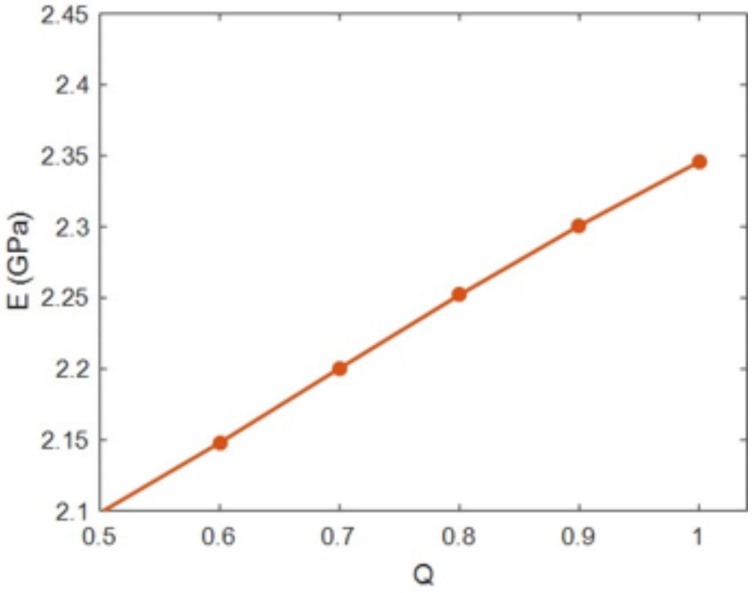

Fig. 5. Correlation of "E" to "Q" by the innovative model.

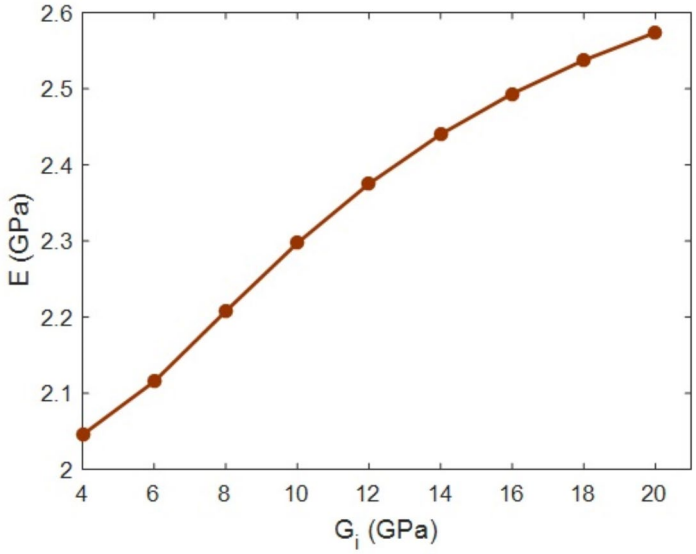

Fig. 6. Estimations of the system's modulus at several points of interfacial shear modulus using the progressive model.

The modulus linearly relates to the HNT weight fraction, and a higher HNT content usually makes a tougher sample.

Since HNTs are significantly stronger than the polymer media, a higher modulus for the system is expected by using a higher content of HNTs. In fact, a high amount of HNTs significantly reinforces the samples because the polymer medium is much poorer than the HNTs, and therefore, HNTs play a reinforcing character in the system. A small quantity of HNTs cannot strengthen the samples since the system comprises a significant concentration of a poor polymer medium. All earlier models have considered the filler concentration as the driving force for the nanocomposite's performance because the exceptional features of nanoparticles such as HNTs considerably manipulate the performance of the samples[27,53–55]. Therefore, the progressed model appropriately handles the inspiration of HNT concentration on the modulus of the system.

Figure 8 depicts the association of the stiffness with the HNT length. $l = 500$ nm produces the lowest modulus of 2 GPa, while the maximum stiffness is 3.16 GPa at $l = 3000$ nm. So, longer HNTs make a tougher nanocomposite, and HNT length directly governs the modulus. Short HNTs cannot reinforce the samples

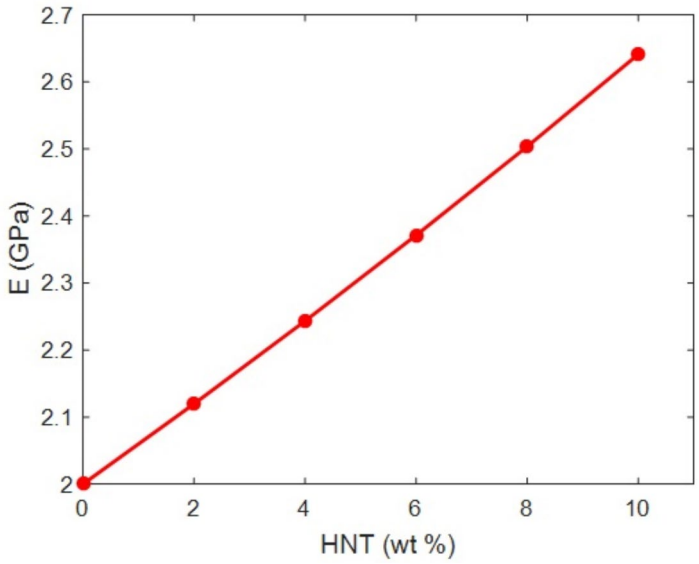

Fig. 7. Correlation of nanocomposite's modulus to HNT weight%.

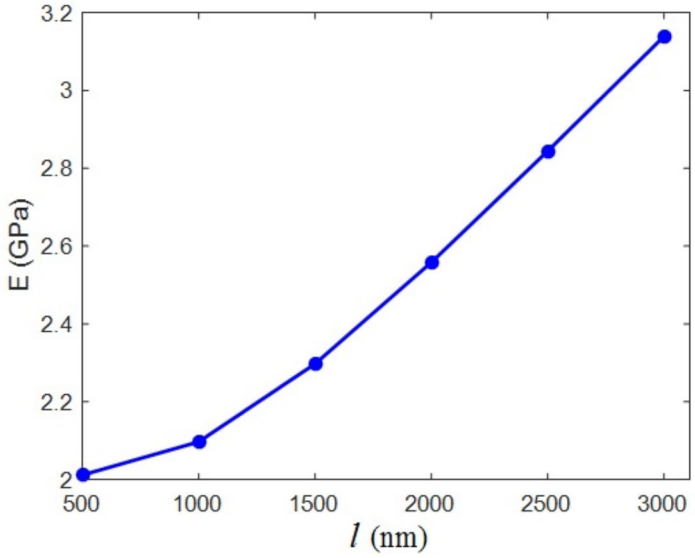

Fig. 8. Significance of HNT length on the "E".

because $l = 500$ nm harvests a modulus of 2 GPa, which is equal to the modulus of the polymer matrix ($E_m = 2$ GPa is assumed in all calculations). Accordingly, the application of long HNTs is essential to stiffen the samples. Additionally, the HNT length of 3000 nm maximizes the modulus to 3.16 GPa, the highest value reported in this paper. Consequently, the HNT length is the most critical parameter for managing the reinforcement of the system, assuming an imperfect interphase.

HNT length has no influence on the "L_c" based on Eq. 1, but it directly changes the "Q" (Eq. 2). This means that longer HNTs cause more efficient stress transferring in nanocomposites. Moreover, Eqs. 4 and 5 demonstrate that longer HNTs produce higher values of the operative aspect ratio and operational concentration of the nanofiller. This shows that long HNTs increase the effectiveness of stress transferring, aspect ratio, and filler amount. Therefore, long HNTs undoubtedly promote the reinforcing of samples. Conversely, short HNTs deteriorate adequate levels for stress transferring, aspect ratio, and concentration of filler, which expectedly weaken reinforcing. These observations endorse the suitability of the advanced model to predict the stiffness at various extents of the HNT length.

Figure 9 reveals the association of the composite's modulus with the HNT radius. The modulus improves to 2.7 GPa at a HNT radius of 20 nm, whereas $R = 60$ nm weakens the modulus of the nanocomposites to 2.04 GPa.

These calculations establish an opposite link among the modulus of the samples and the HNT radius. Slimmer HNTs produce a stiffer system, but thicker HNTs deteriorate the stiffness of nanocomposites. The results show that thick HNTs ($R=60$ nm) are ineffective on the sample's modulus since the modulus is relatively identical to the polymer modulus ($E_m = 2$ GPa is considered). The modulus of the system inconstantly changes with the HNT radius, and narrower HNTs produce better results.

Slim HNTs yield a low range for "L_c" (Eq. 1), which enhances "Q" (Eq. 3), reduces the operative inverse aspect ratio (Eq. 4), and grows the operational filler fraction (Eq. 5). Hence, narrower HNTs produce a powerful interphase section, increasing the effective stress transferring in the system. Additionally, slim HNTs enhance the efficiencies of the aspect ratio and concentration in the samples. Obviously, slim HNTs are appropriate for enhancing the efficiencies of both filler and nearby interphases in the system, increasing the reinforcing. In contrast, thick HNTs enlarge the "L_c", which deteriorates the "Q" and the effective ranges of the filler aspect ratio and filler volume fraction. Accordingly, dense HNTs worsen the productivities of nanoparticles and the interphase zones in the samples, weakening the system's reinforcement. Based on these findings, it can be concluded that the HNT radius adversely manipulates the system's stiffness, ratifying the novel model.

Figure 10 expresses the yields of the novel model at some values of the HNT modulus. $E_f = 80$ GPa causes a stiffness of 2.53 GPa, although the modulus reduces to 2.13 GPa at a HNT modulus of 220 GPa. These results demonstrate an adverse link between the moduli of the samples and HNT. A poor modulus of the HNTs produces a sturdier nanocomposite. However, tough HNTs stiffen the samples. The HNT modulus linearly reduces the nanocomposite's modulus at $E_f < 140$ GPa, but a further increase of the HNT modulus only insignificantly reduces the modulus of the samples. This plot demonstrates that low-modulus HNTs are desirable to reinforce the HNT-based system.

The HNT modulus directly controls the "L_c" based on Eq. 1. Thus, a higher modulus of HNT broadens the "L_c", which deteriorates the stress transferring efficiency in the samples (Q in Eq. 3). Moreover, a longer "L_c" obtained by stiffer HNTs diminishes the actual aspect ratio and real concentration of the nanofiller (Eqs. 4 and 5). These data reveal that stiffer HNTs detrimentally control the stress transferring and the efficiencies of the nanofiller and interphase section in the samples. As a result, stiffer HNTs produce poorer nanocomposites. In contrast, poor HNTs shorten the "L_c", intensifying the stress shifting and the competencies of nanoparticles and nearby interphase in the samples. Clearly, poor HNTs advantageously reinforce the samples based on the progressive model. This result does not agree with the reported results of the earlier models for the modulus of the nanocomposites[56–58] because stiffer HNTs typically yield a stiffer sample. However, the former models suppose a flawless interphase in the samples, while the current model considers a defective interphase section in which "L_c" plays a main character in the reinforcing. Thus, the novel model accurately links the modulus to the HNT modulus by considering a defective interphase zone.

Conclusions

In this paper, "L_c" was expressed, and its roles in the operative inverse aspect ratio, operative HNT concentration, and "Q" were explained. Also, the Hui-Shia model was expanded by assuming an imperfect interphase in the HNT-based system. Slimmer HNTs, longer HNTs, higher interfacial shear modulus, and shorter "L_c" produce a higher "Q". "L_c" adversely manipulates the "φ_{eff}", while a higher "Q" causes a greater "φ_{eff}". The original Hui-Shia model overpredicts the moduli of samples due to the assumption of perfect interphase. In contrast, an acceptable agreement between experimental and theoretical values supports the accuracy of the developed

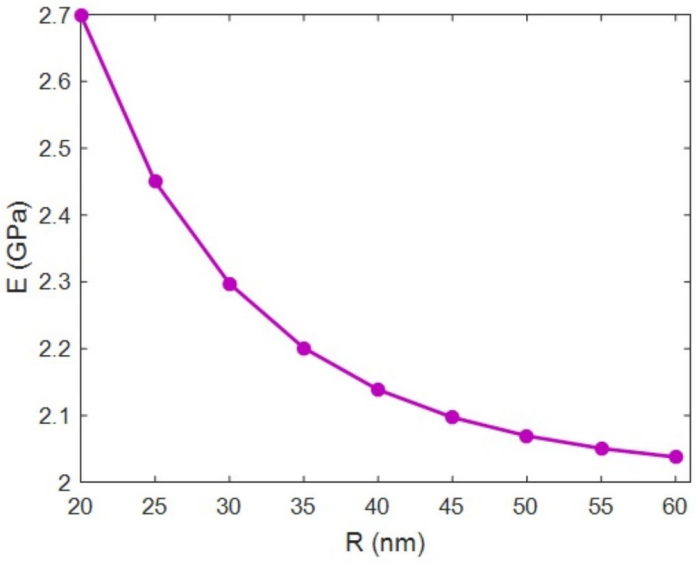

Fig. 9. Variation of stiffness by "R" by the proposed model.

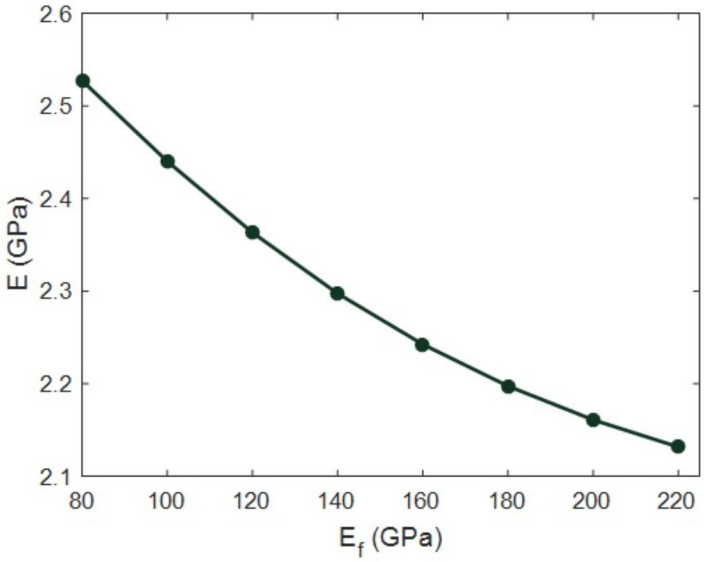

Fig. 10. A relation between the moduli of nanocomposites and HNTs produced by an advanced model.

model. Additionally, calculations of "G_i", "L_c", and "Q" for the examples support the accuracy of the novel model. There is a reverse relation between the modulus of the samples and "L_c". Meanwhile, a higher "Q" and a greater interfacial shear modulus produce a stiffer sample. The stiffness linearly relates to the HNT weight fraction, and a higher HNT concentration usually reinforces the system. $l = 500$ nm yields the lowest modulus of 2 GPa, while the modulus is maximum as 3.16 GPa at $l = 3000$ nm. Moreover, there is a converse connection between the modulus of samples and HNT radius, and a HNT with $R = 60$ nm is unsuccessful in toughening the composites. Hence, thinner and larger HNTs result in a tougher nanocomposite, and HNT length is the most significant factor in manipulating the rigidity of the system. The results reveal an opposite linkage between the moduli of the system and the HNTs. This output contradicts earlier predictions because the previous models supposed a flawless interphase, while the developed model assumes an incomplete interphase.

Data availability

The data that support the findings of this study are available on request from corresponding author.

Received: 15 April 2023; Accepted: 23 September 2024
Published online: 05 October 2024

References

1. Jin, X. et al. An eco-friendly and effective approach based on bio-based substances and halloysite nanotubes for fire protection of bamboo fiber/polypropylene composites. *J. Mater. Res. Technol.* **17**, 3138–3149 (2022).
2. Al-Gaashani, R., Zakaria, Y., Gladich, I., Kochkodan, V. & Lawler, J. XPS, structural and antimicrobial studies of novel functionalized halloysite nanotubes. *Sci. Rep.* **12**(1), 21633 (2022).
3. Eivazzadeh-Keihan, R. et al. Fabrication of a magnetic alginate-silk fibroin hydrogel, containing halloysite nanotubes as a novel nanocomposite for biological and hyperthermia applications. *Sci. Rep.* **12**(1), 15431 (2022).
4. Ghiyasiyan-Arani, M. & Salavati-Niasari, M. Decoration of green synthesized S, N-GQDs and CoFe2O4 on halloysite nanoclay as natural substrate for electrochemical hydrogen storage application. *Sci. Rep.* **12**(1), 8103 (2022).
5. Zare, Y. & Rhee, K. Y. Development of a model for modulus of polymer halloysite nanotube nanocomposites by the interphase zones around dispersed and networked nanotubes. *Sci. Rep.* **12**(1), 1–12 (2022).
6. Boraei, S. B. A. et al. Osteogenesis capability of three-dimensionally printed poly (lactic acid)-halloysite nanotube scaffolds containing strontium ranelate. *Nanatechnol. Reviews.* **11**(1), 1901–1910 (2022).
7. Prashantha, K., Schmitt, H., Lacrampe, M-F. & Krawczak, P. Mechanical behaviour and essential work of fracture of halloysite nanotubes filled polyamide 6 nanocomposites. *Compos. Sci. Technol.* **71**(16), 1859–1866 (2011).
8. Pan, S., Guo, Y., Chen, Y. & Cakmak, M. Kinetics of electric field induced vertical orientation of halloysite nanotubes in photocurable nanocomposites. *Nanoscale Adv.* **1**(9), 3521–3528 (2019).
9. Cheng, C., Song, W., Zhao, Q. & Zhang, H. Halloysite nanotubes in polymer science: purification, characterization, modification and applications. *Nanatechnol. Rev.*. **9**(1), 323–344 (2020).
10. Zubkiewicz, A. et al. Ethylene vinyl acetate copolymer/halloysite nanotubes nanocomposites with enhanced mechanical and thermal properties. *J. Appl. Polym. Sci.* **137**(38), 49135 (2020).
11. Toplosky, V. et al. Mechanical and thermal properties of glass reinforced composites. *IEEE Trans. Appl. Supercond.* **32**(6), 1–5 (2022).
12. Hoque, M. S. & Dolez, P. I. Aging of high-performance fibers used in firefighters' protective clothing: state of the knowledge and path forward. *J. Appl. Polym. Sci.* **140**(32), e54255 (2023).
13. Peng, T. et al. Study of the fatigue behavior of the unidirectional zylon/epoxy composite used in pulsed magnets. *IEEE Trans. Appl. Supercond.* **30**(4), 1–5 (2020).
14. Niu, R. et al. Aging effect of Zylon. *IEEE Trans. Appl. Supercond.* **28**(3), 1–4 (2017).

15. Zubkiewicz, A. et al. Comparing multi-walled carbon nanotubes and halloysite nanotubes as reinforcements in EVA nanocomposites. *Materials*. **13**(17), 3809 (2020).
16. Tang, Y. et al. Effects of unfolded and intercalated halloysites on mechanical properties of halloysite–epoxy nanocomposites. *Compos. Part A: Appl. Sci. Manuf.* **42**(4), 345–354 (2011).
17. Prashantha, K., Lacrampe, M. F. & Krawczak, P. Highly dispersed polyamide-11/halloysite nanocomposites: Thermal, rheological, optical, dielectric, and mechanical properties. *J. Appl. Polym. Sci.* **130**(1), 313–321 (2013).
18. Aguiar, R., Miller, R. E. & Petel, O. E. Microstructural evidence of the toughening mechanisms of polyurethane reinforced with halloysite nanotubes under high strain-rate tensile loading. *Sci. Rep.* **11**(1), 13161 (2021).
19. Zare, Y. & Rhee, K. Y. Expansion of Takayanagi model by interphase characteristics and filler size to approximate the tensile modulus of halloysite-nanotube-filled system. *J. Mater. Res. Technol.* **16**, 1628–1636 (2022).
20. Zare, Y. & Rhee, K. Y. An innovative model for conductivity of graphene-based system by networked nano-sheets, interphase and tunneling zone. *Sci. Rep.* **12**(1), 1–9 (2022).
21. Zare, Y. & Rhee, K. Y. Electrical conductivity of graphene-containing composites by the conduction and volume share of networked interphase and the properties of tunnels applicable in breast cancer sensors. *J. Mater. Sci.* **57**(37), 17637–17648 (2022).
22. Zare, Y. & Rhee, K. Y. Crucial interfacial shear strength to consider an imperfect interphase in halloysite-nanotube-filled biomedical samples. *J. Mater. Res. Technol.* **19**, 3777–3787 (2022).
23. Zare, Y., Rhee, K. Y. & Park, S-J. Progressing of a power model for electrical conductivity of graphene-based composites. *Sci. Rep.* **13**(1), 1596 (2023).
24. Mohammadpour-Haratbar, A., Zare, Y. & Rhee, K. Y. Simulation of electrical conductivity for polymer silver nanowires systems. *Sci. Rep.* **13**(1), 5 (2023).
25. Hassanzadeh-Aghdam, M. K., Mahmoodi, M. J. & Ansari, R. Creep performance of CNT Polymer nanocomposites-An emphasis on viscoelastic interphase and CNT agglomeration. *Compos. Part. B: Eng.* **168**, 274–281 (2019).
26. Hassanzadeh-Aghdam, M. K., Ansari, R. & Mahmoodi, M. J. Thermo-mechanical properties of shape memory polymer nanocomposites reinforced by carbon nanotubes. *Mech. Mater.* **129**, 80–98 (2019).
27. Zamanian, M., Ashenai Ghasemi, F. & Mortezaei, M. Interphase characterization and modeling of tensile modulus in epoxy/silica nanocomposites. *J. Appl. Polym. Sci.* **138**(5), 49755 (2021).
28. Msekh, M. A. et al. Fracture properties prediction of clay/epoxy nanocomposites with interphase zones using a phase field model. *Eng. Fract. Mech.* **188**, 287–299 (2018).
29. Amraei, J., Jam, J. E., Arab, B. & Firouz-Abadi, R. D. Modeling the interphase region in carbon nanotube-reinforced polymer nanocomposites. *Polym. Compos.* **40** (S2), E1219–E34 (2019).
30. Shahrokh, A. & Fakhrabadi, M. M. S. Effects of copper nanoparticles on elastic and thermal properties of conductive polymer nanocomposites. *Mech. Mater.* **160**, 103958 (2021).
31. Zare, Y., Rhee, K. Y. & Park, S-J. Predictions of micromechanics models for interfacial/interphase parameters in polymer/metal nanocomposites. *Int. J. Adhes. Adhes.* **79**, 111–116 (2017).
32. Zare, Y. & Rhee, K. Y. Prediction of tensile modulus in polymer nanocomposites containing carbon nanotubes (CNT) above percolation threshold by modification of conventional model. *Curr. Appl. Phys.* **17**(6), 873–879 (2017).
33. Arjmandi, S. K., Khademzadeh Yeganeh, J., Zare, Y. & Rhee, K. Y. Development of Kovacs model for electrical conductivity of carbon nanofiber–polymer systems. *Sci. Rep.* **13**(1), 7 (2023).
34. Ansari, R. & Hassanzadeh-Aghdam, M. Micromechanical investigation of creep-recovery behavior of carbon nanotube-reinforced polymer nanocomposites. *Int. J. Mech. Sci.* **115**, 45–55 (2016).
35. Maghsoudlou, M. A., Isfahani, R. B., Saber-Samandari, S. & Sadighi, M. Effect of interphase, curvature and agglomeration of SWCNTs on mechanical properties of polymer-based nanocomposites: experimental and numerical investigations. *Compos. Part. B Eng.* **175**, 107119 (2019).
36. Rostami, M., Mohseni, M. & Ranjbar, Z. An attempt to quantitatively predict the interfacial adhesion of differently surface treated nanosilicas in a polyurethane coating matrix using tensile strength and DMTA analysis. *Int. J. Adhes. Adhes.* **34**, 24–31 (2012).
37. Luo, Y., Zhao, Y., Cai, J., Duan, Y. & Du, S. Effect of amino-functionalization on the interfacial adhesion of multi-walled carbon nanotubes/epoxy nanocomposites. *Mater. Des.*. **33**, 405–412 (2012).
38. Zare, Y. Effects of interphase on tensile strength of polymer/CNT nanocomposites by Kelly–Tyson theory. *Mech. Mater.* **85**, 1–6 (2015).
39. Lazzeri, A. & Phuong, V. T. Dependence of the Pukánszky's interaction parameter B on the interface shear strength (IFSS) of nanofiller-and short fiber-reinforced polymer composites. *Compos. Sci. Technol.* **93**, 106–113 (2014).
40. Hui, C. & Shia, D. Simple formulae for the effective moduli of unidirectional aligned composites. *Polym. Eng. Sci.* **38** (5), 774–782 (1998).
41. Zare, Y. & Rhee, K. Y. Advanced Kolarik model for the modulus of a nanocomposite system reinforced by halloysite nanotubes and interphase zone. *Polym. Compos.* (2022).
42. Zare, Y., Rhee, K. Y. & Park, S-J. Tensile Modulus of Polymer Halloysite Nanotube systems containing filler–interphase networks for Biomedical requests. *Materials*. **15**(13), 4715 (2022).
43. Zare, Y. & Rhee, K. Y. Simulation of tensile modulus of polymer carbon nanotubes nanocomposites in the case of incomplete interfacial bonding between polymer matrix and carbon nanotubes by critical interfacial parameters. *Polymer*. **191**, 122260 (2020).
44. Zare, Y. & Rhee, K. Y. The mechanical behavior of CNT reinforced nanocomposites assuming imperfect interfacial bonding between matrix and nanoparticles and percolation of interphase regions. *Compos. Sci. Technol.* **144**, 18–25 (2017).
45. Lecouvet, B., Horion, J., D'haese, C., Bailly, C. & Nysten, B. Elastic modulus of halloysite nanotubes. *Nanotechnology*. **24**(10), 105704 (2013).
46. Fornes, T. & Paul, D. Modeling properties of nylon 6/clay nanocomposites using composite theories. *Polymer*. **44**(17), 4993–5013 (2003).
47. Kundalwal, S. & Kumar, S. Multiscale modeling of stress transfer in continuous microscale fiber reinforced composites with nano-engineered interphase. *Mech. Mater.* **102**, 117–131 (2016).
48. Budarapu, P., Kumar, S., Prusty, B. G. & Paggi, M. Stress transfer through the interphase in curved-fiber pullout tests of nanocomposites. *Compos. Part. B: Eng.* **165**, 417–434 (2019).
49. Handge, U. A., Hedicke-Höchstötter, K. & Altstädt, V. Composites of polyamide 6 and silicate nanotubes of the mineral halloysite: influence of molecular weight on thermal, mechanical and rheological properties. *Polymer*. **51**(12), 2690–2699 (2010).
50. Marset, D. et al. Injection-molded parts of partially biobased polyamide 610 and biobased halloysite nanotubes. *Polymers*. **12**(7), 1503 (2020).
51. Qiu, K. & Netravali, A. N. Halloysite nanotube reinforced biodegradable nanocomposites using noncrosslinked and malonic acid crosslinked polyvinyl alcohol. *Polym. Compos.* **34**(5), 799–809 (2013).
52. Wu, W., Cao, X., Zhang, Y. & He, G. Polylactide/halloysite nanotube nanocomposites: Thermal, mechanical properties, and foam processing. *J. Appl. Polym. Sci.* **130**(1), 443–452 (2013).
53. Deng, F. & Zheng, Q-S. An analytical model of effective electrical conductivity of carbon nanotube composites. *Appl. Phys. Lett.* **92**(7), 071902 (2008).
54. Ghasemi, R. et al. A hybrid mathematical modeling strategy for controlling the mechanical performance of polyethylene/poly (ethylene-co-vinyl acetate)/Nanoclay cast films. *Polym. Test.* 106089. (2019).

55. Drozdov, A. D. & Christiansen, J. Micromechanical modeling of barrier properties of polymer nanocomposites. *Compos. Sci. Technol.* **189**, 108002 (2020).
56. Takayanagi, M., Uemura, S. & Minami, S. Application of equivalent model method to dynamic rheo-optical properties of crystalline polymer. *J. Polym. Sci. Part C Polym. Sympos. Wiley Online Libr.* 113–22 (1964).
57. Ji, X. L., Jiao, K. J., Jiang, W. & Jiang, B. Z. Tensile modulus of polymer nanocomposites. *Polym. Eng. Sci.* **42**(5), 983 (2002).
58. Ouali, N., Cavaillé, J. & Perez, J. Elastic, viscoelastic and plastic behavior of multiphase polymer blends. *Plast. Rubber Compos. Process. Appl. (UK).* **16**(1), 55–60 (1991).

Author contributions
Y.Z. prepared the main text. M.T.M. edited and improved the language of full paper. K.Y.R. revised the paper.

Funding
No funding was received.

Declarations

Competing interests
The authors declare no competing interests.

Additional information
Correspondence and requests for materials should be addressed to Y.Z. or K.Y.R.

Reprints and permissions information is available at www.nature.com/reprints.

Publisher's note Springer Nature remains neutral with regard to jurisdictional claims in published maps and institutional affiliations.